ACS Energy LETTERS

Cite This: ACS Energy Lett. 2019, 4, 2287−2294

http://pubs.acs.org/journal/aelccp

LETTER

Tandem Cuprous Oxide/Silicon Microwire Hydrogen-Evolving Photocathode with Photovoltage Exceeding 1.3 V

Wouter Vijselaar,[†] Pramod Patil Kunturu,[†] Thomas Moehl,[‡] S. David Tilley,*[,‡] and Jurriaan Huskens*[,†]

[†]Molecular Nanofabrication Group, MESA + Institute for Nanotechnology, Faculty of Science and Technology, University of Twente, P.O. Box 217, 7500 AE Enschede, The Netherlands

[‡]Department of Chemistry, University of Zurich, Winterthurerstrasse 190, CH-8057 Zurich, Switzerland

Supporting Information

ABSTRACT: Large research efforts have been devoted to optimizing the output of earth-abundant photoabsorbers in solar-to-fuel (S2F) devices. Here, we report a Cu_2O/Ga_2O_3 heterojunction/Si microwire photocathode with an underlying buried radial Si p−n junction, which achieves efficient light harvesting across the visible spectrum to over 600 nm, reaching an external quantum yield for hydrogen generation close to 80%, with a photocurrent onset above +1.35 V vs RHE, a photocurrent density of ∼10 mA/cm^2 at 0 V vs RHE, and an ideal regenerative efficiency of 5.51%. We show step-by-step the effects of every photocathode design element (i.e., Si p−n junction, Cu_2O layer thickness, microwire length, microwire pitch, etc.) on the overall efficiency of our final microwire Si/Cu_2O photocathode by comparing every addition to a baseline Cu_2O photocathode. Lastly, we show a stable operation exceeding 200 h at a bias potential of +1.0 V vs RHE, with an average current density of 4.5 mA/cm^2.

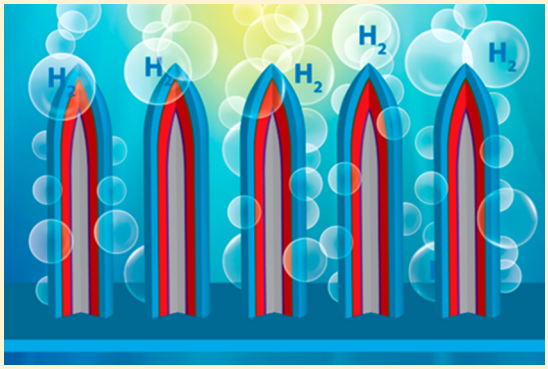

Solar-to-fuel (S2F) is the concept of turning solar energy into a storable fuel in an integrated process. To fabricate a fully integrated, efficient S2F device based on photoelectricity, a single or set of semiconductors must be combined with a proper electrocatalyst. Many single semiconductors are investigated as possible candidates for a photoanode (e.g., Fe_2O_3,[1−3] $BiVO_4$,[4−6] WO_3,[7,8] TiO_2,[9−12] or ZnO[13−15]) or photocathode (e.g., III−V systems,[12] CuO,[16,17] Cu_2O,[18] Si,[19,20] or SiC[21]). However, to date, not a single semiconductor produces both a high photocurrent and enough photovoltage to drive a solar fuel reaction (e.g., production of hydrogen (H_2) and oxygen (O_2)) at an acceptable efficiency.

Fountaine et al. and others showed that a combination of semiconductors with bandgaps of approximately 1.8 and 1.0 eV would give theoretically the highest overall efficiency.[22−25] In an ideal case, each material creates an equal current density (i.e., current matching), and an enhanced photovoltage (V_{oc}) is achieved when the stack is in series. Key considerations in selecting the appropriate materials are photon-to-electron conversion and efficient charge transport across all layers, in order to convert the electrons to hydrogen. A possible combination of materials could be cuprous oxide (Cu_2O) in series with silicon (Si) because they have bandgaps of 2.0 and 1.1 eV, respectively. Both materials are extensively investigated as materials in photovoltaic (PV) cells,[26−31] are earth-abundant, are nontoxic, and are relatively cost-effective to produce. However, a directly coupled tandem cell between Si and Cu_2O has never been investigated. Furthermore, both materials have their own drawbacks, which need to be addressed to improve the overall efficiency for a possible tandem cell. A notable feature for all of the electrodeposited Cu_2O systems, whether used as a photocathode or in a solar cell, is the poor conversion of photons with wavelengths of 500−600 nm due to the mismatch between the absorption depth of the photons and the diffusion length of the photogenerated electrons as a result of the relatively high acceptor concentration in electrodeposited films. Luo et al. surpassed this problem by the fabrication of Cu_2O nanowires, which greatly enhanced the current density up to 9 mA/cm^2 at 0 V vs RHE.[32] Pan et al. improved this and reported recently the best oxide photocathode known today with a Cu_2O/Ga_2O_3 heterojunction, which achieves a photocurrent onset over 1 V

Received: July 1, 2019
Accepted: August 26, 2019
Published: August 26, 2019

DOI: 10.1021/acsenergylett.9b01402
ACS Energy Lett. 2019, 4, 2287−2294

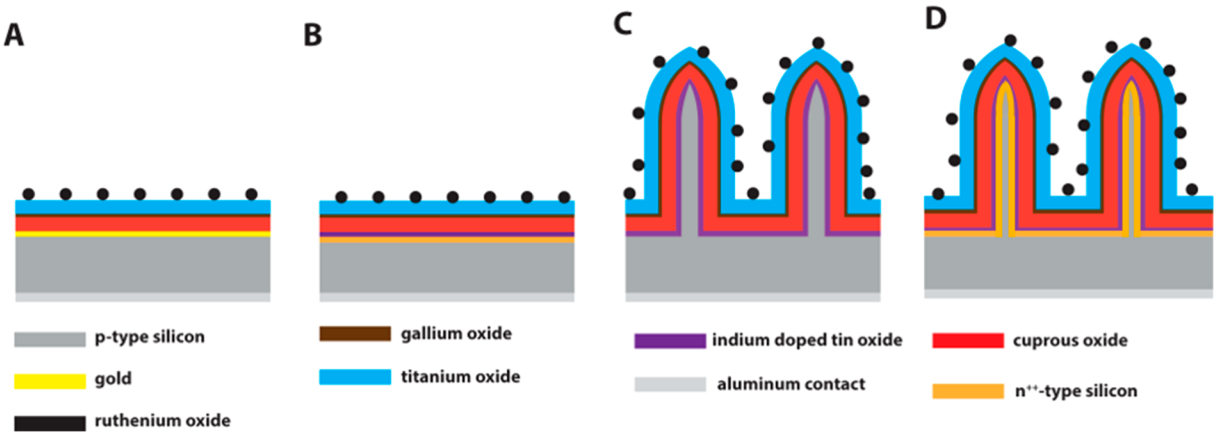

Figure 1. Schematic representation of the different device layer architectures (not to scale). (A) Si substrate (i.e., not used as a photoabsorber) with a layer of gold (150 nm), electrodeposited Cu_2O (200 nm), an emitter of Ga_2O_3 (20 nm), a passivation layer of TiO_2 (100 nm), and a RuO_x catalyst (~2 nm). (B) Planar tandem stack of a Si substrate with a planar p−n junction, ITO (75 nm)/Au particles (5 nm), electrodeposited Cu_2O (150 nm), an emitter of Ga_2O_3 (20 nm), a passivation layer of TiO_2 (100 nm), and a RuO_x catalyst (~2 nm). (C) Si microwire array (15 μm in length), without a p−n junction, with ITO (75 nm)/Au particles, electrodeposited Cu_2O (200 nm), an emitter of Ga_2O_3 (20 nm), a passivation layer of TiO_2 (100 nm), and a RuO_x catalyst (~2 nm). (D) Si microwire array (15 μm in length) containing a radial p−n junction, with ITO (75 nm)/Au particles, electrodeposited Cu_2O (200 nm), an emitter of Ga_2O_3 (20 nm), a passivation layer of TiO_2 (100 nm), and a RuO_x catalyst (~2 nm).

vs RHE and a photocurrent density of ~10 mA/cm^2 at 0 V versus RHE.[33] The smaller energy band offset and favorable band alignment (conduction band) between the Cu_2O and Ga_2O_3 layers diminishes interfacial recombination.[33−36] As a result, the energy for the splitting of the quasi-Fermi levels between the two oxides is larger, hence leading to a higher photovoltage. However, Cu_2O nanowires are grown from a thick copper (Cu) film. A residual Cu film remains after fabrication and would block the incoming light for a possible underlying second low bandgap absorber (e.g., Si) that could further increase the overall voltage and therefore overall efficiency of a S2F device. Furthermore, the photovoltage (~1 V) is not enough to produce hydrogen in a standalone configuration. Even with state-of-the-art materials (e.g., Pt as reduction and IrO_x as oxidation catalyst), the overall required voltage to split water is theoretically 1.23 V but practically >1.4 V.[37]

Paracchino et al. have shown that, besides a high photovoltage, also passivation and catalysis are important contributors to a high overall efficiency.[38] They investigated different passivation layer thicknesses of titanium oxide (TiO_2) and found that they could extend the stability significantly. Such a passivation layer is now well understood, and stability is even further increased.[33] To reduce the overpotential for the electrochemical hydrogen evolution reaction, a stable catalyst is required. Tilley et al. showed that one of the best performing and, above all, stable hydrogen evolution catalyst is ruthenium oxide (RuO_x).[39] Furthermore, in order not to obstruct the light absorption of the underlying layers, nanoparticles are easily deposited by galvanostatic photodeposition.[40]

In order to increase the photovoltage, a second semiconductor can be added either behind or in front of the Cu_2O stack. Bismuth vanadate as a high-bandgap photoanode has been used in the literature in combination with a lower-bandgap material (e.g., Cu_2O).[6,33,41] However, the main reason for the low overall performance is the lack of overall photovoltage.[42] The bandgap of Si is almost ideal, according to simulations as stated above. However, planar Si has an inherently high reflectivity (~30%) over a broad spectrum.[43] The reflectivity can be lowered substantially (<1%) by introducing a Si microwire array with a radial p−n junction, and such arrays have proven to be very effective PV cells.[44,45] The microwires mostly improve the overall efficiency by improved charge collection due to the lower reflectivity and thereby increase the current density. Furthermore, in a tandem cell (e.g., in combination with Cu_2O), Si microwires with a junction can increase the photovoltage of the overall stack. However, direct coupling to Cu_2O has never been shown.

Here we show a geometry for a S2F device that is based on tapered Si microwire arrays to overcome the aforementioned problems (i.e., low light absorption and photovoltage of solely Cu_2O).[46] We present the realization and stability of a microwire Si/Cu_2O tandem cell with a radial p−n junction in the Si microwires. We show that the addition of Si microwires enhances the overall absorption of the Cu_2O stack. Furthermore, the introduction of an underlying radial Si p−n junction increases the overall photovoltage. In order to show the addition of each aspect of the device, we compare the stacks with and without a microwire architecture and with and without a junction in the Si. In this manner, we can deconvolute the influence of every step. Additionally, we investigated the roles of ALD-grown *n*-Ga_2O_3, TiO_2 overlayers, and RuO_x as a cocatalyst in aiding protection from the electrolyte environment and PEC performance. Lastly, we optimized the Cu_2O layer thickness, and the pitch and height of the Si microwires, in order to obtain the highest overall photoconversion efficiency, photovoltage, and current density.

We fabricated four different types of photocathodes to investigate the effect of every change in the stack. Figure 1 is a schematic representation of the different stacks that we are comparing throughout this Letter. The sample depicted in Figure 1A is used as a baseline, which is fabricated as described in the literature.[47] Hereafter, a planar buried p−n junction in the Si is introduced, Figure 1B, to assess the impact of the junction on the produced photovoltage by the underlying Si. Therefore, the solid Au layer in Figure 1A is replaced by a transparent ITO/Au nanoparticle layer, similar to the transparent FTO/Au layer as described by Dias et al.[47] Lastly, Si

DOI: 10.1021/acsenergylett.9b01402
ACS Energy Lett. 2019, 4, 2287−2294

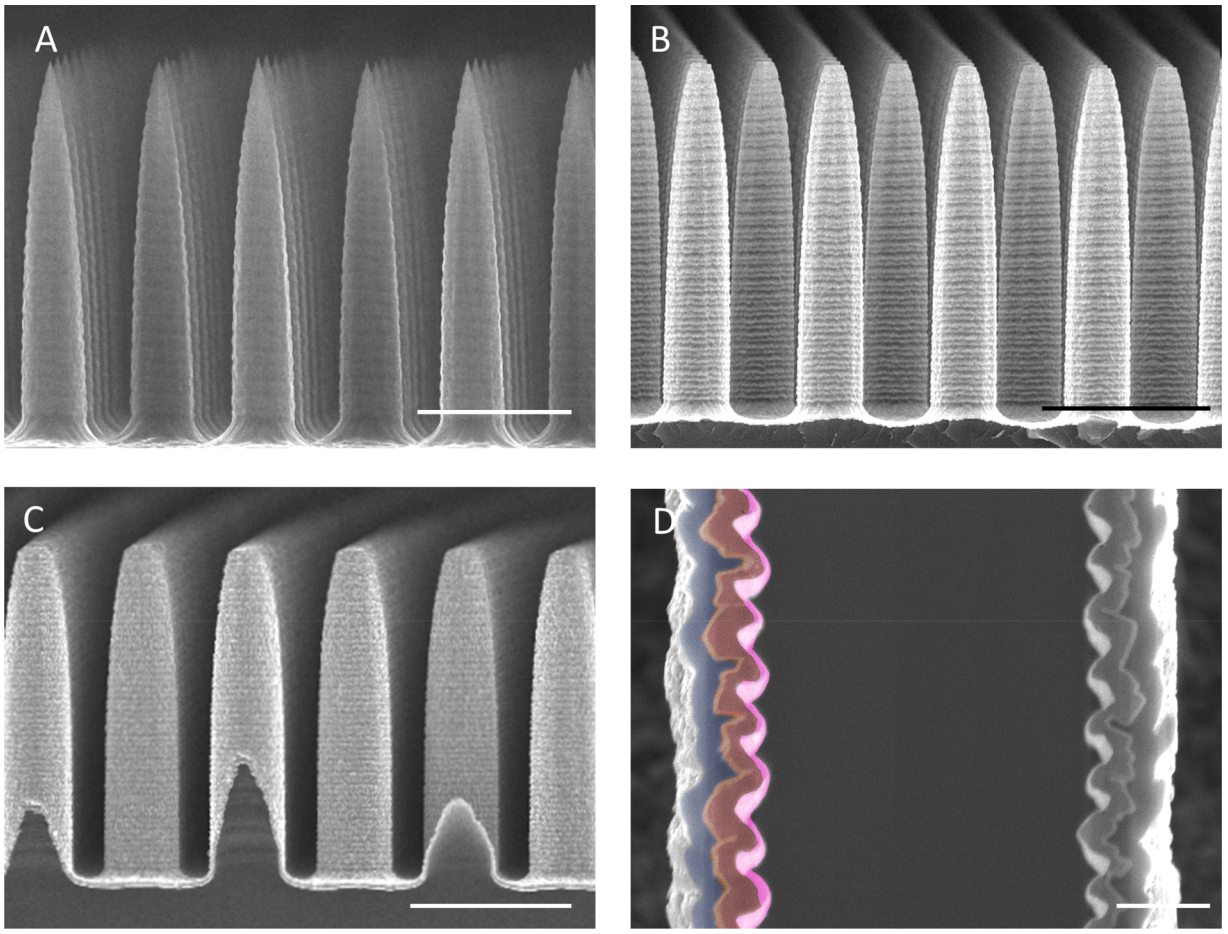

Figure 2. HR-SEM images of the microwire array samples after each of the main process steps of the fabrication process: (A) after the wet-etch step to taper the Si microwires, (B) after sputtering of the ITO/Au layer over the microwires, (C) after the electrodeposition of Cu_2O, and (D) after completing the whole fabrication process and cutting (by FIB) a microwire in the length direction. In (D), the left-hand side is false-colored, ITO/Au (pink), Cu_2O (red), Ga_2O_3 (orange), and TiO_2 (blue). The scale bars in (A−C) are 5 μm; that in (D) is 500 nm.

microwires are introduced in the stack of materials from Figure 1B to obtain stacks without (Figure 1C) and with (Figure 1D) a radial p−n junction. Therefore, we can assess the contributions of the additions of the microwire and the junction separately.

For the structured samples, we etched straight Si microwires, with a width of 4 μm, by deep reactive ion etching (DRIE), and we tapered the microwires by a Si slow etchant (RSE-100). We and others have shown before that sputtering of materials on high-aspect-ratio microwires creates an inhomogeneous layer.[7,45] The latter is solved by tapering the Si microwires; thereby, the microwire top does not form a shadow effect on the lower parts. Also, we taper the microwires to improve the light absorption properties by reducing the reflectivity. The height and pitch of microwires are known to have an effect on the light absorption capabilities.[44,48,49] Therefore, different bare Si microwire arrays with a pitch in the range of 4−24 μm have been fabricated, and with a height varying between 0 (planar, i.e., no microwires) up to 15 μm. We introduced a homogeneous p−n junction into the Si, both in flat and in the microwire samples (Figure 1B,D). A layer of phosphorus oxide was created by depositing a spin-on dopant (SOD). After a short low-temperature drying step, a thermal drive-in diffusion process was carried out to introduce the P dopant into the silicon at 900 °C for 15 min under nitrogen flow. The junction depth was determined by the concentration of dopant and was measured to be around 900 nm.

Electrodeposition of Cu_2O on Si requires the presence of Au for uniform nucleation. On the reference stack, a 200 nm layer of Au was sputtered (Figure 1A). Au was used to form an ohmic contact to the Cu_2O and to direct the growth of Cu_2O in the ⟨111⟩ direction, which is known to have the highest electron conductivity as compared to the other direction.[50] This was followed by electrodeposition of ∼200 nm of Cu_2O, whereby the thickness was controlled by the deposition time. A 20 nm heterogeneous emitter of gallium oxide (Ga_2O_3) and a 100 nm passivation/protection layer of titanium oxide (TiO_2) were both deposited by atomic layer deposition (ALD), and finally, a ruthenium oxide (RuO_x) hydrogen evolution catalyst was deposited by galvanostatic photodeposition.[39]

To use the underlying Si substrate as a photoabsorber (Figure 1B,D), the Au layer needs to be transparent. Therefore, the Au layer in Figure 1A was replaced by sputtering 75 nm of indium-doped tin oxide (ITO) directly followed by sputtering ∼5 nm of Au nanoparticles onto planar Si (Figure 1B) or microwired Si (Figure 1C,D). Because the Au is being sputtered, it does not form a continuous layer, but nanoparticulate islands are formed instead.[47] The transparent Au-nanoparticle-containing layer is referred to as ITO/Au throughout the rest of the paper. Hereafter, we introduce the

DOI: 10.1021/acsenergylett.9b01402
ACS Energy Lett. 2019, 4, 2287−2294

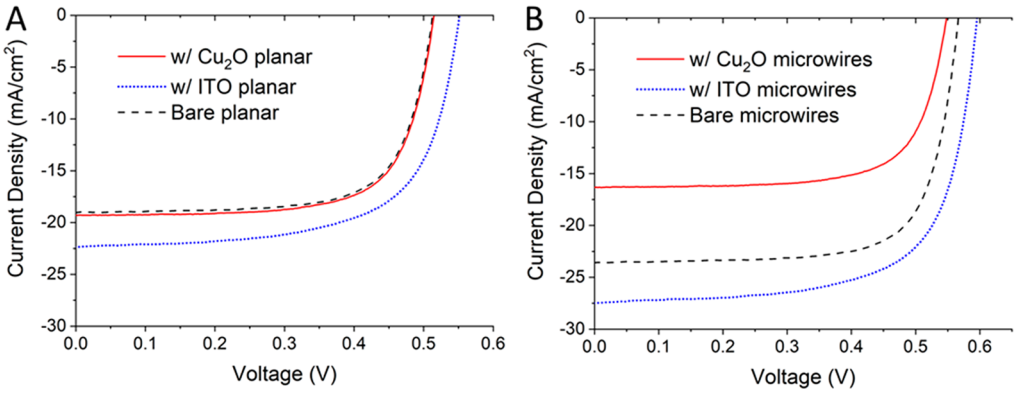

Figure 3. $J-V$ characteristics for dry Si PV cells: (A) planar and (B) microwires, with or without the different overlayers: bare (dashed), with ITO/Au (blue, dotted), and with an additional Cu_2O layer on top of the ITO/Au layer (red, solid).

same $Cu_2O/Ga_2O_3/TiO_2/RuO_x$ layer stack as described above for the reference sample.

We used a mixed ITO/Au layer as a tunnel junction to stimulate conformal growth of the Cu_2O while maintaining a transparent oxide conductor underneath of the stack. The idea was adapted from Dias et al., who used a transparent layer of FTO/Au as the substrate for the oxide growth.[47] Here we show that the same is possible on ITO/Au. The growth was investigated by X-ray diffraction (XRD); see Figure S1. The addition of the Au particles acts clearly as a growth director in the ⟨111⟩ direction, promoting columnar growth of the Cu_2O layer.[47] The columnar morphology is also visualized by HR-SEM (see Figure S2), and the growth of the Cu_2O was found to be linear with time (~6 nm/min).

The layer thickness of the Cu_2O layer on the microwire samples was controlled by applying the same current density as that for a planar sample but increasing the deposition time according to the increased absolute geometric surface area due to the addition of the Si microwires. Table S1 shows the time factor for microwires with a length of 10 μm and for different pitches. The thickness of the deposited Cu_2O layer was investigated by HR-SEM by a cross section, as shown in Figure S3. Here two time equivalents are shown of Figure S2A,B, and the observed thicknesses correspond reasonably well to the thicknesses, as expected for a planar surface.

Figure 2 shows SEM images after each of the main process steps to fabricate the device in Figure 1D. After DRIE, the sample was immersed in a slow Si etching solution (RSE-100) for a short period of time to taper the microwires (Figure 2A). Upon sputtering of ITO, the brightness of the SEM image increased due to improved conductivity (Figure 2B). Due to the tapering of the microwires, the ITO layer is more conformal over the microwires as compared to that without tapering.[7,45] Additionally, Au was sputtered over the sample, which forms most likely islands on top of the ITO layer not visible in the HR-SEM images.[18,47] Because the ITO/Au layer is conducting and the electrodeposition process is mass-transport-limited, a conformal layer of Cu_2O was deposited over the microwires (Figures 2C and S3). Furthermore, the conformality of the complete stack of materials was investigated by cutting a finished microwire along the z-direction by focused ion beam (FIB) etching; see Figure 2D. The left-hand side is false-colored (as by the legend in Figure 2) to aid identification of each of the layers. The ITO layer is present completely over the Si microwire; however, within the crests of the Si microwire (caused by the Bosch etching process), less ITO is present due to the fact that it has been sputtered. Despite the inhomogeneity of the ITO layer, all of the consecutive layers are conformal and not hindered by the scalloping of the Si microwires. Especially the thin Ga_2O_3 layer is conformal over the complete structure. The TiO_2 layer fills the remaining crests and smoothes the outside of the whole microwire.

The influence of the addition of Si microwires on the light absorption capabilities of solely the Cu_2O and ITO/Au layers can be indirectly assessed by investigating the loss in light absorption of the underlying Si PV cell. We tested the underlying Si PV cell after the addition of the ITO/Au layer because it is known that ITO also acts as a passivation and antireflective layer for Si.[45] Therefore, to evaluate the absorption of light in the Cu_2O layer, we quantified the changes in light absorption due to the addition of the ITO/Au layer and after the subsequent addition of the Cu_2O layer, with and without Si microwires (geometry as shown in Figure 1B,1D but with Cu_2O as the outer layer), as depicted in Figure 3. The different measurement setups are illustrated including contacting points to the potentiostat in Figure S4 for both a planar and microwire setup and both with and without the different overlayers.

Figure 3A shows that for a planar Si PV cell with ITO on top both the J_{sc} and V_{oc} increase due to the addition of the ITO/Au layer. This increase is most likely due to the passivation and antireflection properties of the layer. After the addition of a Cu_2O layer on a planar PV cell (with the ITO/Au layer), the V_{oc} and J_{sc} of the Si PV cell decreased again. The J_{sc} decreased by 4.5 mA/cm^2 due to the Cu_2O layer when compared with only an ITO layer. The decrease in V_{oc} of the planar Si PV cell is most likely due to the decrease in light intensity on the cell.

The $J-V$ characteristics of bare Si microwires with a radial p−n junction were also measured (see Figure 3B). Both the V_{oc} and J_{sc} showed an increase with respect to a bare planar sample, which is due to the increase in light absorption capabilities of the Si microwires.[51] When applying an ITO layer over the Si microwires, the J_{sc} and V_{oc} increased even further due to the antireflection and passivation properties. Upon addition of a Cu_2O layer, a substantial decrease in J_{sc} was observed. The J_{sc} for a Si microwire PV cell with Cu_2O decreased by ~11 mA/cm^2, which indicates that the Cu_2O layer absorbs even more sunlight when placed over the microwire sample as compared to the planar sample. Yet, the remaining current density (approximately 17 mA/cm^2) is sufficiently high for the Si substrate not to become the limiting

DOI: 10.1021/acsenergylett.9b01402
ACS Energy Lett. 2019, 4, 2287−2294

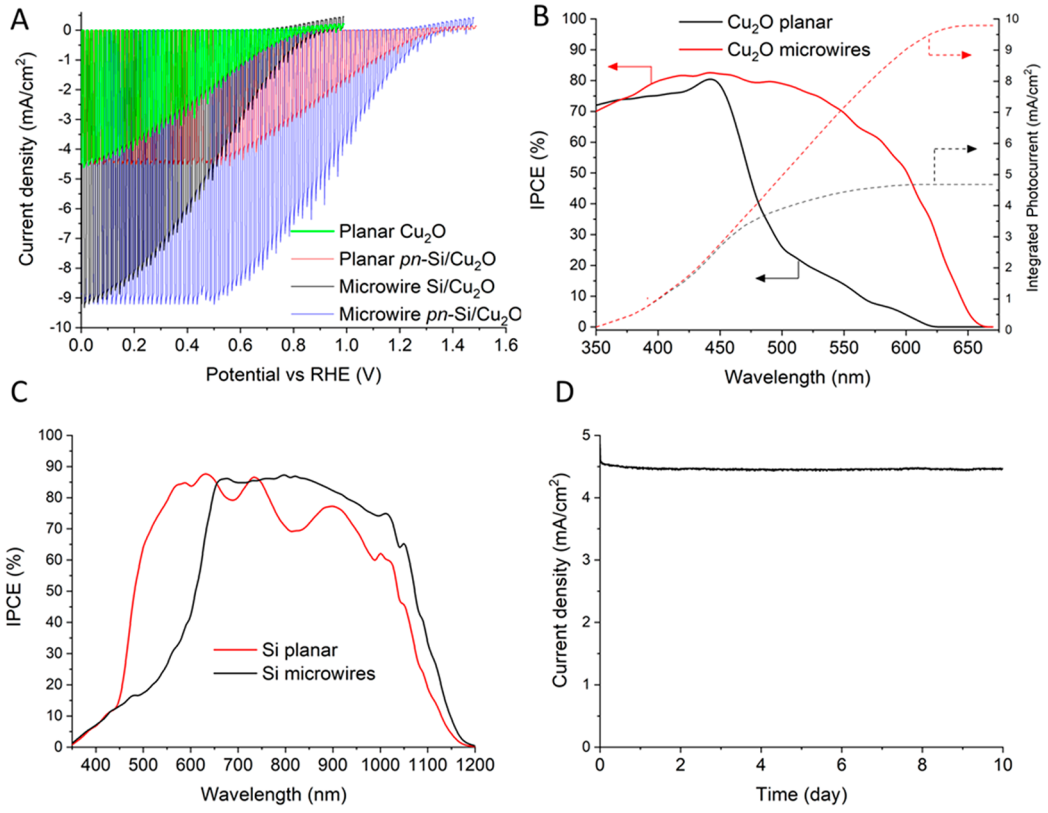

Figure 4. (A) PEC response under simulated AM 1.5G chopped illumination for planar Si/Cu_2O (green), planar Cu_2O tandem with an underlying Si p−n junction (red), Cu_2O on a microwire substrate (black), and Cu_2O tandem on microwires with underlying p−n junction (blue) photocathodes (geometries as shown in Figure 1A−D, respectively; the setup is shown in Figure S6). (B) Corresponding wavelength-dependent IPCE measurements for Si/Cu_2O planar and a microwire Cu_2O top absorber with a buried radial p−n junction (as in Figure 1B,D). (C) Corresponding wavelength-dependent IPCE measurements for Si/Cu_2O planar and a microwire Si bottom absorber with a buried radial p−n junction (as in Figure 1B,D). (D) PEC stability test of a Cu_2O tandem cell on microwires (Figure 1D) at a fixed bias of 1 V versus RHE under illumination, with continuous stirring and a platinum mesh used as a counter electrode. All measurements were performed at pH 5.0 using a combination of 0.5 M Na_2SO_4 and 0.1 M phosphate solution using a three-electrode configuration.

layer in the overall current density of the device because the maximum theoretical photocurrent of the Cu_2O is limited to 14.5 mA/cm^2.[32]

Second, we fabricated microwire samples with varying pitches, microwire heights, and Cu_2O thicknesses (geometry as shown in Figure 1D but with Cu_2O as the outer layer). We screened these parameters to find the optimum current density output (Figure S5). The Cu_2O layer thickness was optimized with respect to its short-circuit current density (J_{sc}); see Figure S5A. It was found that a Cu_2O layer thickness of ∼150−200 nm was optimal to achieve the highest J_{sc}. Most likely, a thinner layer does not absorb all of the incoming sunlight and therefore has a lower current density output. A thicker layer, however, will absorb more of the incoming light, but electrons generated deep within the Cu_2O layer will not reach the surface because of recombination within the Cu_2O layer due to the limited minority carrier diffusion length of maximally ∼200 nm.[32,52,53]

The J_{sc} was measured for the microwire arrays with different heights (from 0 to 15 μm), and microwires with a length of 10 μm gave the highest output (see Figure S5B). Lastly, the microwires' pitch (core to core distance) was varied from 4 to 24 μm. Here it was found that a smaller pitch led to a higher J_{sc}; see Figure S5C. The highest tested pitch (24 μm) approached the performance of a planar surface, and the microwires did not provide any gain to the light absorption anymore. The pitch of the microwire arrays cannot be smaller than 4 μm because the wire width (>2 μm) and combined layer thickness (of ITO, Cu_2O, and TiO_2) would become higher than the pitch. Therefore, Si microwire arrays with a pitch of 4 μm, a height of 10 μm, and a Cu_2O layer thickness of ∼200 nm were considered optimal.

Figure 4A shows the PEC performance of the four fabricated Si/Cu_2O photocathode samples (Figure 1A−D) measured in a three-electrode configuration using the Si/Cu_2O photocathodes as the working electrode, a platinum mesh as the counter electrode, and Ag/AgCl as the reference electrode (see Figure S6) under chopped light conditions. As a reference, we also provide the data obtained under continuous illumination and in the dark (Figure S7). All of the photocathodes were compared regarding the relevant values (i.e., J_{ph} or J_{sc}, V_{oc}, fill factor (FF), and efficiency (η)), which are tabulated in Table 1. The efficiency was calculated as an ideal regenerative cell

Table 1. Overview of the Characteristics of the Different Cu_2O Photocathodes

	V_{oc} (V)	J_{sc} (mA/cm^2)	FF (%)	η_{irc} (%)
planar Si/Cu_2O	0.88	−4.51	32.08	1.25
planar pn-Si/Cu_2O	1.36	−4.43	44.31	2.70
microwire Si/Cu_2O	0.92	−9.23	28.81	2.52
microwire pn-Si/Cu_2O	1.34	−9.52	45.07	5.51

DOI: 10.1021/acsenergylett.9b01402
ACS Energy Lett. 2019, 4, 2287−2294

(IRC) efficiency, which is described by an equation similar to that used to describe the efficiency of a PV device, see eq 1

$$\eta_{IRC} = \frac{V_{oc} J_{ph} (E_{H_2/H^+}) FF}{P_{in}} \quad (1)$$

The values of FF, V_{oc}, and J_{ph} in eq 1 were referenced to the equilibrium potential of the half-reaction being performed at the photocathode (the hydrogen evolution reaction), and P_{in} is the light power input (AM 1.5G, 100 mW/cm^2). This equation has been chosen following Coridan et al., who proposed a unified method of comparing photoelectrodes for PEC.[54] Preconditions for the application of this formula is the (reasonable) assumption that the electrochemical potential under actual hydrogen evolution conditions is at 0 vs RHE and, furthermore, that the overpotential for the RuO_x as a hydrogen evolution catalyst is not too high (which has been investigated in detail for (photo)cathodes by Pastor et al.).[55] Our optimized baseline sample (see Figure 1A) is depicted in green. From Figure 4A, it becomes clear that the introduction of solely microwire structures underneath of the Cu_2O (i.e., Figure 1C) has no noticeable influence on the generated photovoltage. However, by introducing a planar p−n junction (i.e., Figure 1B) underneath of the complete stack, the photovoltage is increased to ∼1.36 V, which is ∼500 mV higher than our baseline (Figure 1A). The latter is in agreement with the dry PV cell measurement, as observed in Figure 3A. Furthermore, by introducing both Si microwires and a radial p−n junction (i.e., Figure 1D), the photovoltage is again increased to ∼1.34 V (see Figure 4A). All four measurements in Figure 4A show fluctuations in the photocurrent density due to vigorous hydrogen bubble evolution. Especially the planar pn-Si/Cu_2O (red) and microwire pn-Si/Cu_2O (blue) samples show a slight decrease in current density in the plateau region. Furthermore, a decrease in current density at around ∼450 mV is observed for the microwire pn-Si/Cu_2O sample (blue). This is most likely due to clinging of bubbles to the photocathode surface, which decreases the effective surface area until the bubbles are released.

Incorporating a p−n junction into the Si does not alter the light absorption capabilities of the Cu_2O layer. This is clearly visible when comparing both planar samples (with geometries as shown in Figure 1A,B), without (green) and with (red) a buried junction (see Figure 4A), which shows that the J_{sc} values are virtually the same. From Figure 3, it is clear that the Cu_2O layer is the photocurrent-limiting layer because the underlying planar Si PV cell still generates 19 mA/cm^2, which is far more than the ∼4.5 mA/cm^2 produced in the PEC cell. However, the short-circuit density increased from 4.5 to 9.2 mA/cm^2 upon going from a flat to a microwired sample (Figure 1A,C). The J_{sc} is, for the devices in series, limited by the Cu_2O. The increase in J_{sc} of the microwired structure is reflected in the increased "parasitic" absorption and reduction of J_{sc} with the Cu_2O layer on the dry Si PV cell, as discussed above for Figure 3.

The increase in current density is also well understood by measurements of the incident photon-to-current conversion efficiency (IPCE) of both a planar Cu_2O (Figure 1A) and a microwired pn-Si/Cu_2O (Figure 1C) photocathode (Figure 4B). Electrodeposited Cu_2O on a planar substrate absorbs light well up to 450 nm, beyond which the absorptivity drops rapidly to zero. The integrated photocurrent from the IPCE data combined with the AM 1.5G solar spectrum corresponds well to the value of the photocurrent presented in Figure 4A and to the current loss for a planar PV cell shown in Figure 3A. The IPCE for a microwire sample shows a broad plateau response across a wide spectral range. This broad response enhances the current density output tremendously, as is visible for both the integrated photocurrent and the output shown in Figure 4A, and this behavior is in accordance with the current decrease shown in Figure 3B. The increase in the IPCE values (Figure 4B), as achieved by microstructuring, resulted in an overall improved J_{sc} value. Our results are in agreement with those of Pan et al.,[33] who have shown that implementing a 3D nanostructure of Cu_2O yields a broad absorption from the UV to 650 nm. The IPCE of the bottom Si absorber is also affected by the structuring (see Figure 4C). Oscillations are visible at higher wavelengths. These are most likely due to interference between the different planar layers. These oscillations are not visible with the microwired samples due to scattering of the light within the highly structured surface. We show here that the strategy of implementing the microwire 3D structure into electrodeposited Cu_2O can be utilized to harvest the red part of the incoming light. The overall regenerative efficiency is a comprehensive manner to assess the overall effect of an increase of both the V_{oc} and J_{sc}. The η_{irc} of the planar tandem PEC cell (Figure 1B) doubles with respect to our baseline planar photocathode (Figure 1A), from 1.25 to 2.70%, due to the increase in photovoltage. By incorporating the Cu_2O microwires (Figure 1C), the η_{irc} again doubles as compared to our baseline planar photocathode, from 1.25 to 2.52%. However, combining both systems (Figure 1D) leads to both an increased overall J_{sc} due to the Cu_2O microwires and a maximum obtainable V_{oc} due to the underlying microwire Si PV cell, thereby increasing the overall efficiency from 1.25 to a record 5.51%.

Lastly, we have examined the TiO_2 protection layer deposited by ALD for suppressing photocorrosion. The ALD-deposited conformal TiO_2 layer protects the Cu_2O/Ga_2O_3 buried junction from direct contact with the electrolyte and transports the photogenerated electrons to the electrolyte where hydrogen evolution takes place (Figure S8). A PEC stability test under bias at 1 V vs RHE showed hardly any degradation over time (Figure 4D). Only during the first day was a slight fall in current density observed, which leveled off thereafter. Operation over a period of 10 days consecutively showed an excellent stability even under load. With more than 200 h, this is the longest stability test reported for such Cu_2O photocathodes, to the best of our knowledge. The stable operation of the Si/Cu_2O photocathode protected by TiO_2 is attributed to three main factors: (i) the ALD-deposited TiO_2 film is highly stable in aqueous media;[12,33] (ii) there is no change in oxidation state of the titania film; and (iii) the HER catalyst (RuO_x) remains attached in a stable manner throughout the operation.

In summary, we have demonstrated a benchmark tandem Si/Cu_2O microwire photocathode featuring a current density of 9.5 mA/cm^2 at 0 V versus RHE and 4.5 mA/cm^2 at +1 V versus RHE and a photovoltage of ∼1.4 V utilizing a microstructured Cu_2O absorber, a Ga_2O_3 emitter layer, a TiO_2 protection layer, and a RuO_x HER catalyst. The IPCE curves showed a plateau between 300 and 600 nm for a microstructured Cu_2O layer while dropping sharply in the region between 400 and 500 nm for a planar sample. The microstructuring doubled the overall current density. Making

DOI: 10.1021/acsenergylett.9b01402
ACS Energy Lett. 2019, 4, 2287−2294

use of the transparent interlayer of ITO/Au nanoparticles, a buried p−n junction in Si can be further employed. This extra junction pushed the obtainable open-circuit potential from ∼1 to ∼1.4 V. All-in-all, the better light absorption and the additional voltage from the underlying buried junction increased the regenerative efficiency of 1.25% for a planar Cu_2O photocathode to 5.51% for a microwired pn-Si/Cu_2O one. The stability test at 1 V vs RHE showed great promise to use the described geometry in a S2F device because the stability did not change over the course of 10 days even under load (at 1 V vs RHE). In conclusion, our results provide rational design strategies for making efficient Cu_2O-based photocathodes and push the frontier of PEC water splitting.

■ ASSOCIATED CONTENT

Supporting Information

The Supporting Information is available free of charge on the ACS Publications website at DOI: 10.1021/acsenergylett.9b01402.

XRD patterns, HR-SEM images, area enhancement calculations, SEM images, schematic illustrations of experimental setups, plots of current density vs geometric parameters, PEC response plots, band diagram illustrations, schematic overview of the fabrication process, and the experimental section (PDF)

■ AUTHOR INFORMATION

Corresponding Authors

*E-mail: j.huskens@utwente.nl (J.H.).
*E-mail: david.tilley@chem.uzh.ch (S.D.T.).

ORCID

S. David Tilley: 0000-0002-7542-1147
Jurriaan Huskens: 0000-0002-4596-9179

Notes

The authors declare no competing financial interest.

■ ACKNOWLEDGMENTS

Henk van Wolferen is acknowledged for the FIB experiments, and Mark Smithers is thanked for the HR-SEM images. We thank Prof. Guido Mul for use of the solar simulator. J.H. acknowledges the Institute of Advanced Study, Durham University, UK, for hosting him as a Fellow and for fruitful discussions. This work is part of the research program of the Foundation for Fundamental Research on Matter (FOM, Project 13CO12-2), which is part of The Netherlands Organization for Scientific Research (NWO). P.P.K. is grateful to the Karnataka state government for providing a scholarship under the D Devraj Urs Videshi Vyasanga Vetana scheme. We thank the Swiss National Science Foundation (AP Energy Grant # PYAPP2 160586) and the University of Zurich Research Priority Program (URPP) LightChEC for funding.

■ REFERENCES

(1) Zhong, D. K.; Cornuz, M.; Sivula, K.; Grätzel, M.; Gamelin, D. R. Photo-assisted electrodeposition of cobalt−phosphate (Co−Pi) catalyst on hematite photoanodes for solar water oxidation. *Energy Environ. Sci.* **2011**, *4*, 1759−1764.

(2) Zhong, D. K.; Gamelin, D. R. Photo-electrochemical water oxidation by cobalt catalyst ("Co-Pi")/α-Fe2O3 composite photoanodes: Oxygen evolution and resolution of a kinetic bottleneck. *J. Am. Chem. Soc.* **2010**, *132*, 4202−4207.

(3) Gurudayal; Kumar, M. H.; Wong, L. H.; Barber, J.; Grätzel, M.; Mathews, N.; Sabba, D. Perovskite−Hematite Tandem Cells for Efficient Overall Solar Driven Water Splitting. *Nano Lett.* **2015**, *15*, 3833−3839.

(4) Kim, T. W.; Ping, Y.; Galli, G. A.; Choi, K.-S. Simultaneous enhancements in photon absorption and charge transport of bismuth vanadate photoanodes for solar water splitting. *Nat. Commun.* **2015**, *6*, 8769.

(5) Abdi, F. F.; Firet, N.; Van de Krol, R. Efficient BiVO4 Thin Film Photoanodes Modified with Cobalt Phosphate Catalyst and W-doping. *ChemCatChem* **2013**, *5*, 490−496.

(6) Kim, J. H.; Jo, Y.; Kim, J. H.; Jang, J. W.; Kang, H. J.; Lee, Y. H.; Kim, D. S.; Jun, Y.; Lee, J. S. Wireless Solar Water Splitting Device with Robust Cobalt-Catalyzed, Dual-Doped BiVO4 Photoanode and Perovskite Solar Cell in Tandem: A Dual Absorber Artificial Leaf. *ACS Nano* **2015**, *9*, 11820−11829.

(7) Shaner, M. R.; Fountaine, K. T.; Ardo, S.; Coridan, R. H.; Atwater, H. A.; Lewis, N. S. Photoelectrochemistry of core−shell tandem junction n−p+-Si/n-WO3 microwire array photoelectrodes. *Energy Environ. Sci.* **2014**, *7*, 779−790.

(8) Miecznikowski, K.; Ramirez-Caro, A.; Fiechter, S.; Kulesza, P. J. Enhancement of Water Oxidation at Tungsten Oxide Photoanodes Doped with Borotungstate-Polyanion Modified-Hematite. *Meeting Abstracts* **2015**, *MA2015-01*, 1752.

(9) Li, Z.; Yao, C.; Yu, Y.; Cai, Z.; Wang, X. Highly Efficient Capillary Photoelectrochemical Water Splitting Using Cellulose Nanofiber-Templated TiO2 Photoanodes. *Adv. Mater.* **2014**, *26*, 2262−2267.

(10) Xu, Y.; Melia, M. A.; Tsui, L.-k.; Fitz-Gerald, J. M.; Zangari, G. Laser-Induced Surface Modification at Anatase TiO2 Nanotube Array Photoanodes for Photoelectrochemical Water Oxidation. *J. Phys. Chem. C* **2017**, *121*, 17121−17128.

(11) Butburee, T.; Bai, Y.; Wang, H.; Chen, H.; Wang, Z.; Liu, G.; Zou, J.; Khemthong, P.; Lu, G. Q. M.; Wang, L. 2D Porous TiO2 Single-Crystalline Nanostructure Demonstrating High Photo-Electrochemical Water Splitting Performance. *Adv. Mater.* **2018**, *30*, 1705666.

(12) Bae, D.; Seger, B.; Vesborg, P. C. K.; Hansen, O.; Chorkendorff, I. Strategies for stable water splitting via protected photoelectrodes. *Chem. Soc. Rev.* **2017**, *46*, 1933−1954.

(13) Wang, N.; Liu, M.; Tan, H.; Liang, J.; Zhang, Q.; Wei, C.; Zhao, Y.; Sargent, E. H.; Zhang, X. Compound Homojunction:Heterojunction Reduces Bulk and Interface Recombination in ZnO Photoanodes for Water Splitting. *Small* **2017**, *13*, 1603527.

(14) Lamberti, A.; Gazia, R.; Sacco, A.; Bianco, S.; Quaglio, M.; Chiodoni, A.; Tresso, E.; Pirri, C. F. Coral-shaped ZnO nanostructures for dye-sensitized solar cell photoanodes. *Prog. Photovoltaics* **2014**, *22*, 189−197.

(15) Steinmiller, E. M. P.; Choi, K.-S. Photochemical deposition of cobalt-based oxygen evolving catalyst on a semiconductor photoanode for solar oxygen production. *Proc. Natl. Acad. Sci. U. S. A.* **2009**, *106*, 20633−20636.

(16) Masudy-Panah, S.; Siavash Moakhar, R.; Chua, C. S.; Kushwaha, A.; Dalapati, G. K. Stable and Efficient CuO Based Photocathode through Oxygen-Rich Composition and Au−Pd Nanostructure Incorporation for Solar-Hydrogen Production. *ACS Appl. Mater. Interfaces* **2017**, *9*, 27596−27606.

(17) Septina, W.; Prabhakar, R. R.; Wick, R.; Moehl, T.; Tilley, S. D. Stabilized Solar Hydrogen Production with CuO/CdS Heterojunction Thin Film Photocathodes. *Chem. Mater.* **2017**, *29*, 1735−1743.

(18) Son, M.-K.; Steier, L.; Schreier, M.; Mayer, M. T.; Luo, J.; Grätzel, M. A copper nickel mixed oxide hole selective layer for Au-free transparent cuprous oxide photocathodes. *Energy Environ. Sci.* **2017**, *10*, 912−918.

(19) Oh, J.; Deutsch, T. G.; Yuan, H.-C.; Branz, H. M. Nanoporous black silicon photocathode for H2 production by photoelectrochemical water splitting. *Energy Environ. Sci.* **2011**, *4*, 1690−1694.

(20) Warren, E. L.; McKone, J. R.; Atwater, H. A.; Gray, H. B.; Lewis, N. S. Hydrogen-evolution characteristics of Ni−Mo-coated,

DOI: 10.1021/acsenergylett.9b01402
ACS Energy Lett. 2019, 4, 2287−2294

radial junction, n+ p-silicon microwire array photocathodes. *Energy Environ. Sci.* **2012**, *5*, 9653−9661.
(21) van Dorp, D. H.; Hijnen, N.; Di Vece, M.; Kelly, J. J. SiC: A Photocathode for Water Splitting and Hydrogen Storage. *Angew. Chem., Int. Ed.* **2009**, *48*, 6085−6088.
(22) Walter, M. G.; Warren, E. L.; McKone, J. R.; Boettcher, S. W.; Mi, Q.; Santori, E. A.; Lewis, N. S. Solar water splitting cells. *Chem. Rev.* **2010**, *110*, 6446−6473.
(23) Fountaine, K. T.; Lewerenz, H. J.; Atwater, H. A. Efficiency limits for photoelectrochemical water-splitting. *Nat. Commun.* **2016**, *7*, 13706.
(24) Doscher, H.; Geisz, J. F.; Deutsch, T. G.; Turner, J. A. Sunlight absorption in water - efficiency and design implications for photoelectrochemical devices. *Energy Environ. Sci.* **2014**, *7*, 2951−2956.
(25) Bolton, J. R.; Strickler, S. J.; Connolly, J. S. Limiting and Realizable Efficiencies of Solar Photolysis of Water. *Nature* **1985**, *316*, 495−500.
(26) Zhao, J.; Wang, A.; Altermatt, P. P.; Wenham, S. R.; Green, M. A. 24% efficient perl silicon solar cell: Recent improvements in high efficiency silicon cell research. *Sol. Energy Mater. Sol. Cells* **1996**, *41−42*, 87−99.
(27) Shah, A.; Torres, P.; Tscharner, R.; Wyrsch, N.; Keppner, H. Photovoltaic technology: The case for thin-film solar cells. *Science* **1999**, *285*, 692−698.
(28) Saga, T. Advances in crystalline silicon solar cell technology for industrial mass production. *NPG Asia Mater.* **2010**, *2*, 96−102.
(29) Minami, T.; Nishi, Y.; Miyata, T.; Abe, S. Photovoltaic Properties in Al-doped ZnO/non-doped Zn1-XMgXO/Cu2O Heterojunction Solar Cells. *ECS Trans.* **2013**, *50*, 59−68.
(30) Lee, Y. S.; Heo, J.; Siah, S. C.; Mailoa, J. P.; Brandt, R. E.; Kim, S. B.; Gordon, R. G.; Buonassisi, T. Ultrathin amorphous zinc-tin-oxide buffer layer for enhancing heterojunction interface quality in metal-oxide solar cells. *Energy Environ. Sci.* **2013**, *6*, 2112−2118.
(31) Minami, T.; Nishi, Y.; Miyata, T. Effect of the thin Ga2O3 layer in n+-ZnO/n-Ga2O3/p-Cu2O heterojunction solar cells. *Thin Solid Films* **2013**, *549*, 65−69.
(32) Luo, J.; Steier, L.; Son, M.-K.; Schreier, M.; Mayer, M. T.; Grätzel, M. Cu2O Nanowire Photocathodes for Efficient and Durable Solar Water Splitting. *Nano Lett.* **2016**, *16*, 1848−1857.
(33) Pan, L.; Kim, J. H.; Mayer, M. T.; Son, M.-K.; Ummadisingu, A.; Lee, J. S.; Hagfeldt, A.; Luo, J.; Grätzel, M. Boosting the performance of Cu2O photocathodes for unassisted solar water splitting devices. *Nat. Catal.* **2018**, *1*, 412−420.
(34) Lee, Y. S.; Chua, D.; Brandt, R. E.; Siah, S. C.; Li, J. V.; Mailoa, J. P.; Lee, S. W.; Gordon, R. G.; Buonassisi, T. Atomic Layer Deposited Gallium Oxide Buffer Layer Enables 1.2 V Open-Circuit Voltage in Cuprous Oxide Solar Cells. *Adv. Mater.* **2014**, *26*, 4704−4710.
(35) Wong, T. K. S.; Zhuk, S.; Masudy-Panah, S.; Dalapati, G. K. Current Status and Future Prospects of Copper Oxide Heterojunction Solar Cells. *Materials* **2016**, *9*, 271.
(36) Li, C.; Hisatomi, T.; Watanabe, O.; Nakabayashi, M.; Shibata, N.; Domen, K.; Delaunay, J.-J. Positive onset potential and stability of Cu2O-based photocathodes in water splitting by atomic layer deposition of a Ga2O3 buffer layer. *Energy Environ. Sci.* **2015**, *8*, 1493−1500.
(37) McCrory, C. C.; Jung, S.; Ferrer, I. M.; Chatman, S. M.; Peters, J. C.; Jaramillo, T. F. Benchmarking Hydrogen Evolving Reaction and Oxygen Evolving Reaction Electrocatalysts for Solar Water Splitting Devices. *J. Am. Chem. Soc.* **2015**, *137*, 4347−4357.
(38) Paracchino, A.; Laporte, V.; Sivula, K.; Grätzel, M.; Thimsen, E. Highly active oxide photocathode for photoelectrochemical water reduction. *Nat. Mater.* **2011**, *10*, 456.
(39) Tilley, S. D.; Schreier, M.; Azevedo, J.; Stefik, M.; Graetzel, M. Ruthenium Oxide Hydrogen Evolution Catalysis on Composite Cuprous Oxide Water-Splitting Photocathodes. *Adv. Funct. Mater.* **2014**, *24*, 303−311.
(40) Niu, W.; Moehl, T.; Cui, W.; Wick-Joliat, R.; Zhu, L.; Tilley, S. D. Extended Light Harvesting with Dual Cu_2O-Based Photocathodes for High Efficiency Water Splitting. *Adv. Energy Mater.* **2018**, *8*, 1702323.
(41) Kim, J. H.; Jang, J.-W.; Jo, Y. H.; Abdi, F. F.; Lee, Y. H.; Van de Krol, R.; Lee, J. S. Hetero-type dual photoanodes for unbiased solar water splitting with extended light harvesting. *Nat. Commun.* **2016**, *7*, 13380.
(42) Bornoz, P.; Abdi, F. F.; Tilley, S. D.; Dam, B.; Van de Krol, R.; Graetzel, M.; Sivula, K. A Bismuth Vanadate−Cuprous Oxide Tandem Cell for Overall Solar Water Splitting. *J. Phys. Chem. C* **2014**, *118*, 16959−16966.
(43) Lee, K.; Hwang, I.; Kim, N.; Choi, D.; Um, H.-D.; Kim, S.; Seo, K. 17.6%-Efficient radial junction solar cells using silicon nano/micro hybrid structures. *Nanoscale* **2016**, *8*, 14473−14479.
(44) Elbersen, R.; Vijselaar, W.; Tiggelaar, R. M.; Gardeniers, H.; Huskens, J. Effects of Pillar Height and Junction Depth on the Performance of Radially Doped Silicon Pillar Arrays for Solar Energy Applications. *Adv. Energy Mater.* **2016**, *6*, 1501728.
(45) Vijselaar, W.; Elbersen, R.; Tiggelaar, R. M.; Gardeniers, H.; Huskens, J. Photo-Electrical Characterization of Silicon Micropillar Arrays with Radial p/n Junctions Containing Passivation and Anti-Reflection Coatings. *Adv. Energy Mater.* **2017**, *7*, 1601497.
(46) Dahl, S.; Chorkendorff, I. Solar-fuel generation: Towards practical implementation. *Nat. Mater.* **2012**, *11*, 100−101.
(47) Dias, P.; Schreier, M.; Tilley, S. D.; Luo, J.; Azevedo, J.; Andrade, L.; Bi, D.; Hagfeldt, A.; Mendes, A.; Grätzel, M.; Mayer, M. T. Transparent Cuprous Oxide Photocathode Enabling a Stacked Tandem Cell for Unbiased Water Splitting. *Adv. Energy Mater.* **2015**, *5*, 1501537.
(48) Vijselaar, W.; Westerik, P.; Veerbeek, J.; Tiggelaar, R. M.; Berenschot, E.; Tas, N. R.; Gardeniers, H.; Huskens, J. Spatial Decoupling of Light absorption and Catalytic Activity of NiMo-loaded High-aspect-ratio Silicon Microwire Photocathodes. *Nature Energy* **2018**, *3*, 185−192.
(49) Elbersen, R.; Vijselaar, W.; Tiggelaar, R. M.; Gardeniers, H.; Huskens, J. Fabrication and Doping Methods for Silicon Nano- and Micropillar Arrays for Solar-Cell Applications: A Review. *Adv. Mater.* **2015**, *27*, 6781−6796.
(50) Huang, M. H. Facet-Dependent Optical Properties of Semiconductor Nanocrystals. *Small* **2019**, *15*, 1804726.
(51) Elbersen, R.; Tiggelaar, R. M.; Milbrat, A.; Mul, G.; Gardeniers, H.; Huskens, J. Controlled Doping Methods for Radial p/n Junctions in Silicon. *Adv. Energy Mater.* **2015**, *5*, 1401745.
(52) Zhang, Z.; Dua, R.; Zhang, L.; Zhu, H.; Zhang, H.; Wang, P. Carbon-Layer-Protected Cuprous Oxide Nanowire Arrays for Efficient Water Reduction. *ACS Nano* **2013**, *7*, 1709−1717.
(53) de Jongh, P. E.; Vanmaekelbergh, D.; Kelly, J. J. Cu2O: Electrodeposition and Characterization. *Chem. Mater.* **1999**, *11*, 3512−3517.
(54) Coridan, R. H.; Nielander, A. C.; Francis, S. A.; McDowell, M. T.; Dix, V.; Chatman, S. M.; Lewis, N. S. Methods for Comparing the Performance of Energy-conversion Systems for Use in Solar Fuels and Solar Electricity Generation. *Energy Environ. Sci.* **2015**, *8*, 2886−2901.
(55) Pastor, E.; Le Formal, F.; Mayer, M. T.; Tilley, S. D.; Francàs, L.; Mesa, C. A.; Grätzel, M.; Durrant, J. R. Spectroelectrochemical analysis of the mechanism of (photo)electrochemical hydrogen evolution at a catalytic interface. *Nat. Commun.* **2017**, *8*, 14280.

DOI: 10.1021/acsenergylett.9b01402
ACS Energy Lett. 2019, 4, 2287−2294